Available online at www.sciencedirect.com
ScienceDirect
International Journal of Heat and Mass Transfer 50 (2007) 105–116
International Journal of HEAT and MASS TRANSFER
www.elsevier.com/locate/ijhmt

Thermal damage reduction associated with *in vivo* skin electroporation: A numerical investigation justifying aggressive pre-cooling

S.M. Becker, A.V. Kuznetsov *

North Carolina State University, Mechanical and Aerospace Engineering, Box 7910, Raleigh, NC 27695, United States

Received 26 February 2006; received in revised form 27 June 2006
Available online 1 September 2006

Abstract

Electroporation is an approach used to enhance transdermal transport of large molecules in which the skin is exposed to a series of electric pulses. Electroporation temporarily destabilizes the structure of the outer skin layer, the stratum corneum, by creating microscopic pores through which agents, which ordinarily are unable to pass into the skin, are able to pass through this outer barrier. Of possible concern when exposing biological tissue to an electric field is thermal tissue damage associated with Joule heating. In order to find the electrical and transient thermal solutions associated with this process, this study develops a three-dimensional transient finite-volume composite model of *in vivo* skin electroporation. The electroporation process modeled consists of five 150 ms long DC square wave pulses administered at 1-s intervals with an applied voltage of 400 V. This paper finds that minor thermal influence of the electrode plate and the of a small presence blood vessel have a large impact on thermal damage. An aggressive pre-cooling technique is presented which is shown to dramatically reduce the risk of thermal damage.

Keywords: Skin electroporation; Numerical; Aggressive cooling; Thermal damage; Composite

1. Introduction

Electroporation is a technique in which the cell membrane is altered in order to increase permeability into the cell cytosol by inducing an electric field in which the transmembrane potential exceeds a critical threshold [1–5]. The lipid bilayer matrix of the thin (10–20 μm) outermost layer of the skin, the stratum corneum (SC), acts as a barrier inhibiting transdermal drug delivery. It has been shown that electroporation changes the structure of the SC creating aqueous pores [6–8]. The breakdown of the SC barrier allows for increased molecular transport and radically reduces the electrical resistance of the skin [6,9–12].

In dealing with *in vivo* biological tissues exposed to an electric field it is important to consider the temperature rise associated with Joule heating. The severity of this temperature rise is proportional to pulse length and magnitude and is strongly tied to tissue electrical properties. Experimental results show that transdermal molecular flux rates increase with increased pulse duration and magnitude [13–16]. Experiments involving homogenous tissue electroporation have shown that the success of large molecule gene transfer is strongly tied to the amount of heat generated [17,18]. Extensive and novel numerical studies have been conducted for homogenous tissue cases in which factors influencing thermal responses of electroporation are explored. An innovative application of electroporation is proposed in [19] in which irreversible electroporation is used to induce non-thermal killing of cancerous tissue. In [20] one and two-dimensional finite element models are implemented in order to gain useful insight of the temperature related effects of physical influences such as vasculature, convection, metabolic heat generation, and electrode

* Corresponding author. Tel.: +1 919 515 5292; fax: +1 919 515 7968.
E-mail address: avkuznet@eos.ncsu.edu (A.V. Kuznetsov).

0017-9310/$ - see front matter © 2006 Elsevier Ltd. All rights reserved.
doi:10.1016/j.ijheatmasstransfer.2006.06.030

geometry and spacing. A homogenous tissue model of *in vivo* plate electroporation is developed in [21] in which thermal response to electroporation pulse parameters and vasculature is explored. In [22] the importance of the composite layer representation of skin electroporation is stressed. The purpose of this paper is to not only address factors affecting thermal damage of *in vivo* skin electroporation but also to show that pre-cooling the tissue reduces the risk of thermal damage, allowing the experimentalist to use pulse parameters which increase the likelihood of successful drug delivery.

2. Model geometry

This paper considers external parallel plate electroporation in which the electrodes are in direct contact with the skin. Fig. 1 shows the geometric model representation of the system in which a small section of tissue is raised and two thin electrodes are positioned on either side of the target region (at the axial center of the system). A small blood vessel is modeled running axially through the center of the raised tissue. Table 1 lists the model dimensions used. The coordinate system origin lies at the target region center (the blood vessel center) for the x and y axes, and for the z-axis, along the axial upwind side of the target region entrance. The blood vessel's circular circumference is modeled by a polygon of 16 equal sides. The electrode plates are represented by rectangular bars that act as cooling fins to the electroporated tissue.

A representative composite model is used to depict the skin and underlying tissue layers of the human volar forearm. The outer skin layer, the epidermis, is without vasculature. The previously mentioned outermost layer of the epidermis, the SC, is highly electrically insulative and acts as a protective barrier to the skin preventing molecule transport. The inner skin layer is the highly vascular dermis. The dermal skin blood flow exceeds metabolic requirements and the excess blood flow primarily regulates body temperature [23]. Below the dermis is a thermally insulative fat layer that acts to conserve body heat. The innermost layer is the subcutaneous tissue layer which in this study is modeled as muscle tissue. Fig. 2 shows this composite layer model used to represent the skin and underlying tissue.

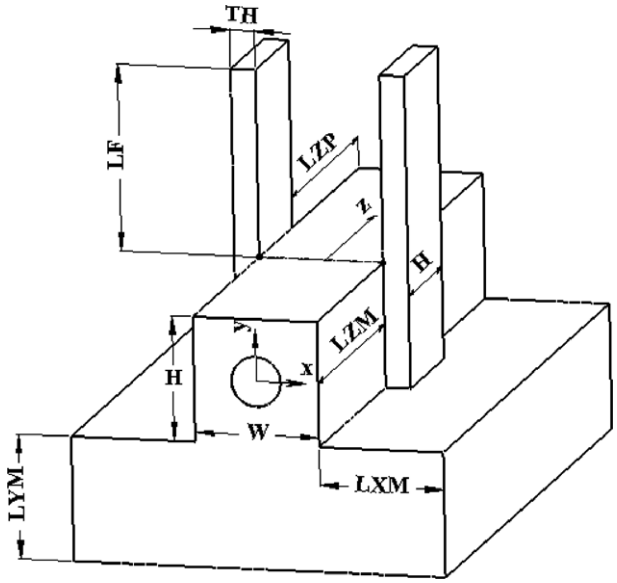

Fig. 1. Model geometry.

Table 1
Model dimensions

Symbol	Description	Value (mm)
R	Blood vessel radius	0, 0.3
W	Electrode spacing	10
H	Electrode face dimension, target region height	10
TH	Electrode thickness	1
LF	Electrode length above target region	100
LZM	Upwind axial length (pre-target region)	15
LZP	Downwind axial length (post-target region)	15
LYM	Vertical depth below target region	9.805
LXM	Horizontal width past target region	8.5

3. Mathematical model

3.1. Thermal energy

In finding the thermal solution, the system is divided into three sub-domains: vessel, composite tissue, and electrode plate.

To represent the composite tissue domain, the Pennes' bioheat equation [24] is used along with an additional source term:

$$\rho_m c_m \frac{\partial T_m}{\partial t} = \nabla \cdot (k_m \nabla T) - \omega_m c_b (T - T_a) + q'''_m + Q_J \qquad (1)$$

where ρ is the density, c is the specific heat, k is the thermal conductivity, T is the temperature, T_a is the arterial temperature, Q_J is the Joule heat generated from the induced electric field, q''' is the metabolic volumetric heat generation, ω_m is the non-directional blood flow associated with perfusion, t is the time, and x, y, and z are the Cartesian coordinate directions. The subscript m refers to one of the four composite tissue layers: stratum corneum (SC), epidermis (ED), dermis (D), subcutaneous fat (F), and subcutaneous muscle tissue (T).

Vascular lock is a phenomenon characterized and termed in [25] in which blood perfusion is obstructed after the application of an electric pulse: after the pulse is administered, blood perfusion is temporarily (depending on pulse severity) stopped. Following these results, in this model the blood perfusion of Eq. (1) is neglected in the target region after the first pulse application:

$$\rho_m c_m \frac{\partial T_m}{\partial t} = \nabla \cdot (k_m \nabla T_m) - A[\omega_m c_b (T_m - T_a)] + q'''_m + Q_J \qquad (2)$$

where $A = \begin{cases} 1 & \text{outside target region} \\ 0 & \text{inside target region} \end{cases}$.

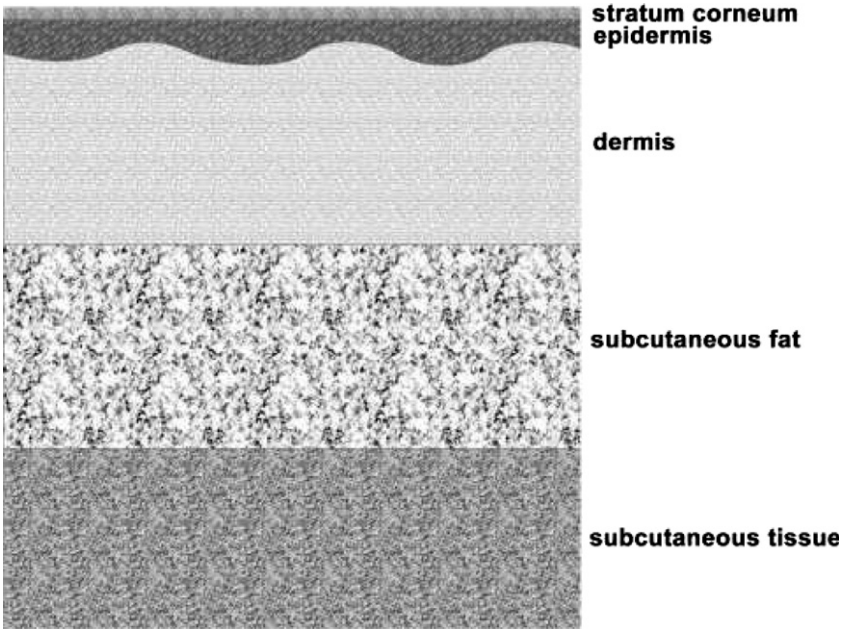

Fig. 2. Composite skin model.

The cases addressed in this study involve the effects associated with the presence of a small blood vessel in the center of the composite tissue domain. To represent the blood vessel domain, the following energy equation is used:

$$\rho_b c_b \left(\frac{\partial T_b}{\partial t} + w \frac{\partial T_b}{\partial z} \right) = \nabla \cdot (k_b \nabla T_b) + Q_J \tag{3}$$

where the subscript b refers to blood parameters, and w is the axial blood velocity. The effects of pulsation resulting from heartbeat are neglected and the blood is treated as a Newtonian fluid. The axial blood flow is assumed to have a parabolic profile and since the coordinate system origin lies in the axial center of the vessel, the blood velocity distribution is defined as:

$$w = 2w_{AV} \left(1 - \frac{(x^2 + y^2)}{R^2} \right) \tag{4}$$

where w_{AV} is the averaged blood velocity.

A representative blood vessel radius of 0.3 mm is used with the corresponding average blood velocity, w_{AV}, of 6 mm/s based on data given in [26]. The vessel wall is assumed to have the same property values as the surrounding tissue. The biological composite tissue and blood properties are presented in Table 2.

The electrode plate section is represented by the transient conduction equation:

$$\rho_e c_e \frac{\partial T_e}{\partial t} = \nabla \cdot (k_e \nabla T_e) \tag{5}$$

where the subscript e refers to electrode plate parameters. Electrode property values are given in Table 3. Parameter temperature dependencies are neglected in this study.

Commonly in parallel plate electroporation a conductive gel is used between the electrodes and the target region, thus in this model electrical and thermal contact resistance at the electrode–tissue interface are neglected.

3.2. Boundary and initial conditions

Initial temperature distributions of the tissue and blood region domains are calculated from the steady state forms of Eqs. (1) and (3) without the induced electric field:

Table 2
Composite tissue and blood properties

			SC	ED	D	F	T	b
Thickness	mm	δ	0.015 [23]	0.035 [23]	1.1 [31]	1.2 [31]	–	–
Thermal conductivity	W/m K	k	0.2 [27]	0.209 [30]	0.293 [30]	0.23 [28]	0.5 [28]	0.572 [28]
Density	kg/m^3	ρ	1500 [28]	1110 [28]	1116 [28]	850 [29]	1040 [28]	1060 [28]
Heat capacity (specific)	J/kg K	c	3600 [29]	3600 [29]	3800 [29]	2300 [29]	3800 [29]	3840 [28]
Perfusion	kg/m^3 s	ω	0	0	2.33 [32]	0.545 [32]	0.695 [32]	–
Metabolic heat generation	W/m^3	q'''	0	0	200 [29]	5 [29]	800 [29]	–
Electrical conductivity	S/m	σ	10^{-5} [28] Pre-breakdown	0.01	0.015	0.02 [28]	0.41 [28]	0.62 [28]

Table 3
Parameter values

ρ_e	Electrode density	7850 kg/m^3
c_e	Electrode specific heat	450 J/kg K
k_e	Electrode thermal conductivity	16 W/m K
T_a	Arterial blood temperature	37°C
T_∞	Ambient temperature	20°C
V_{app}	Applied voltage	400 V

$$0 = \nabla \cdot (k_m \nabla T_m) - \omega_m c_b (T_m - T_a) + q'''_m \tag{6}$$

$$\rho_b c_b w \frac{\partial T_b}{\partial z} = \nabla \cdot (k_b \nabla T_b) \tag{7}$$

Blood perfusion within the target region is not neglected in Eq. (6) and the electrodes are not included in the model for the steady state solution. The electrodes are added to the model at the onset of the first electroporation pulse, and unless otherwise specified are left in contact with the target region for all remaining computations. Initially electrodes are assumed to have the same temperature as the surroundings, T_∞:

$$T_e(x, y, z, 0) = T_\infty \tag{8}$$

The temperature of the lower face of the composite tissue domain is assumed to be equal to the arterial blood temperature, T_a:

$$T_T(x, y_{min}, z, t) = T_a \tag{9}$$

The remaining boundary faces of the composite tissue domain not exposed to the ambient environment are assumed thermally insulated:

$$\begin{aligned} \frac{\partial}{\partial z} T_m(x, y, z_{min}, t) &= \frac{\partial}{\partial z} T_m(x, y, z_{max}, t) \\ &= \frac{\partial}{\partial x} T_m(x_{min}, y, z, t) \\ &= \frac{\partial}{\partial x} T_m(x_{max}, y, z, t) = 0 \end{aligned} \tag{10}$$

The blood vessel inlet temperature is assumed to be equal to T_a while axial thermal conduction at the outlet is neglected:

$$T_b(x, y, z_{min}, t) = T_a \tag{11}$$

$$\frac{\partial}{\partial z} T_b(x, y, z_{max}, t) = 0 \tag{12}$$

Along the outer surface of the composite domain (the SC), a convective flux boundary condition is imposed onto all sides exposed to the ambient air:

$$q'' = h(T_{SC} - T_\infty) = -k_{SC} \left. \frac{\partial T_{SC}}{\partial n} \right|_{surface} \tag{13}$$

where q'' is the heat flux convected from the exposed face, h is the convection coefficient, T_∞ is the ambient air temperature, and n is the normal direction to the surface.

A convective flux boundary condition is imposed onto all electrode sides exposed to the ambient air:

$$q'' = h(T_e - T_\infty) = -k_e \left. \frac{\partial T_e}{\partial n} \right|_{surface} \tag{14}$$

For the electrode plate, the face of the end away from the tissue domain is treated as an insulated fin tip:

$$q'' = 0 = -k_e \left. \frac{\partial T_e}{\partial y} \right|_{tip} \tag{15}$$

The convection coefficient, h, of boundary conditions (13) and (14) is modeled to represent the natural convection of air, and it is solved from:

$$h = \frac{Nu \cdot k_f}{L} \tag{16}$$

where Nu is the average Nusselt number over the face, k_f is the fluid film thermal conductivity, and L is a characteristic length scale defined as: $L = \begin{cases} \text{Vertical} : H_s \\ \text{Horizonal} : \frac{A_s}{P_s} \end{cases}$ where H_s is the vertical surface height, A_s is the horizontal surface area, and P_s is the horizontal surface periphery.

Correlations described in [33] are used to evaluate the averaged Nusselt number, Nu, as follows:

For vertical surfaces:

$$Nu = \left\{ 0.825 + \frac{0.387 \cdot Ra^{1/6}}{[1 + (0.492/Pr)^{9/16}]^{8/27}} \right\}^2 \tag{17}$$

For horizontal surfaces cooling:

$$Nu = 0.54 Ra^{1/4} \tag{18}$$

For the horizontal surfaces heating:

$$Nu = 0.27 Ra^{1/4} \tag{19}$$

Pr is the Prandtl number and Ra is the Rayleigh number which is defined as:

$$Ra = \frac{g\beta(T_s - T_\infty)L^3}{\alpha \nu} \tag{20}$$

where g is gravity, β is the coefficient of volumetric thermal expansion, α is the thermal diffusivity, ν is the kinematic viscosity, and T_s is the surface temperature. The surface temperature value used in Eq. (20) is obtained by averaging the temperature over the surface. The values of the fluid properties k_f, Pr, β, α, and ν are evaluated at the air film temperature, T_f, which is defined as:

$$T_f = \frac{(T_s + T_\infty)}{2} \tag{21}$$

3.3. Electric field power generation

The electrical conductivity of the SC is several orders of magnitude lower than the underlying composite layers. As the barrier function of the SC is destabilized by electroporation induced pore formation, transdermal electric currents are given less resistive routes by which to pass this barrier, thus lowering the effective SC resistivity. Experimentally it has been shown *in vitro* that when exposed to an intense

electric field the electrical resistance of the skin temporarily drops two to three orders of magnitude in a time period of micro to milliseconds depending on pulse intensity and length [6,9,10]. In [14] *in vitro* experiments show that for intense, short pulses the SC resistance drops from 50 kΩ to 60 Ω and with some SC resistance recovery occurring between pulses separated by time periods from 5 s to 5 min. To model the passive breakdown of the SC electrical resistivity, the conductivity of the SC is prescribed a published pre-breakdown value of $\sigma_{SC} = 10^{-5}$ S/m [28] during the first 5 ms of the first electroporation pulse, and thereafter is increased to a value of $\sigma_{SC} = 10^{-2}$ S/m. It is assumed that the electrical properties of the SC do not recover to the pre-pulse values during the 5-s time interval during which the 5 pulses of 150 ms duration are applied. These homogenous effective SC conductivities are used in calculations as it is beyond the scope and purpose of this paper to model localized current passage through the SC. Current passing through normal skin is believed to follow two parallel pathways: one is through the cell matrix composing the SC and the other through skin appendages such as hair follicles and sweat glands [35]. It is beyond the scope of this study to model the local pathways through the skin, so here uniform conductivities are used within composite layers. In [35] it is shown that even at moderate voltages the capacitive charging time associated with non-Ohmic behavior of the skin is very short and may be neglected at times greater than 1 ms. This behavior is neglected in this study.

The lipid bilayer matrix configuration of the SC is without question the greatest contributor to electrical resistance in the skin [23], and it is this layer that undergoes the greatest change in electrical properties during skin electroporation, subsequently making the SC the greatest contributor to overall increase in current density [22]. Furthermore the authors are unaware of any experimental data describing passive electrical property changes in electroporated skin tissue other than that of the SC. For these reasons only the electroporation associated changes in electrical properties of the SC are considered in this study. Epidermal and dermal electrical conductivities given in Table 2 have been chosen to reflect electrical resistance drop with increased depth into the skin [23]. It has been shown that effective electrical resistance of biological tissue decreases with frequency [34], and this paper uses the electrical properties at the low frequency range.

During electroporation the induced electric field causes a temperature rise due to Joule heating. The power supplied is found as follows. The electric potential is solved from the Laplace equation:

$$\nabla \cdot (\sigma_m \nabla \phi) = 0 \tag{22}$$

where ϕ is the electric potential and σ_m is the composite electrical conductivity. This equation is solved using the following boundary conditions: at one electrode the electric potential is zero, while at the other electrode the potential is the same as the applied voltage, V_{app}:

$$\phi\left(-\frac{W}{2}, y, z\right) = 0, \phi\left(\frac{W}{2}, y, z\right) = V_{app} \tag{23}$$

where W is the distance between the electrodes. In this study a Direct current pulse is modeled with an applied voltage value of $V_{app} = 400$ V and a plate spacing of $W = 1$ cm.

All other boundaries of the target area are assumed electrically insulated:

$$\frac{\partial \phi}{\partial n} = 0 \tag{24}$$

where n represents the normal direction to the insulated face.

The power due to Joule heating is then defined as:

$$Q_J = \sigma_m |\nabla \phi|^2 \tag{25}$$

where σ_m is the tissue electrical conductivity. Obviously there is no Joule heating outside the target region or at times during which the electric pulses are not applied.

In [36,37] it is explained that an increase in current density about the electrode perimeter often occurs as a result of low electrode impedance coupled with large tissue resistance. This paper neglects such edge effects. The remaining system parameter values are given in Table 3.

3.4. Damage evaluation

Thermal damage occurs when tissue temperature is elevated over a period of time. In [38] a thermal dose estimate is proposed to quantify thermal damage in part so that damage may be compared between different time-at-temperature situations. In this model, the level of damage is described in a time–temperature relation as in [38] in which thermal damage is represented in minutes of exposure at 43 °C by

$$\mathrm{EM}_{43} = \int R^{(43-T)}\,\mathrm{d}t \tag{26}$$

where $R = \begin{cases} 0.25 & T < 43\,^{\circ}\mathrm{C} \\ 0.5 & T > 43\,^{\circ}\mathrm{C} \end{cases}$ and T is the temperature. In this model the thermal dose is calculated beginning with the onset of the first applied electric pulse.

The sensitivity of biological tissue to thermal dose varies significantly between animal species and specific tissue type [39]. While it is reported for pig muscle, fat and skin tissues that significant chronic histological damage and gross appearance thermal dose thresholds begin at values $\mathrm{EM}_{43} > 80$ min [39], values of EM_{43} in the range 240–340 min have been used to denote permanent thermal tissue damage for muscle, liver and kidney tissues [26,38–40].

4. Discretization and solution procedure

The computational domain is discretized using a variable rectangular grid consisting of 112,760 cells for cases without a blood vessel and 158,720 cells for the case with a blood vessel. A fully implicit finite volume approach is

used to solve Eqs. (1)–(3), (5)–(7), (22), and (25). Temperature, T, and Joule heat, Q_J, are evaluated at the cell centers while the electric potential, ϕ, is evaluated at the cell boundaries. A global 5 ms time step is used for transient Eqs. (1)–(3), and (5). Interface conductivity is represented by a harmonic mean similar to that described in [41], while a resistor representation is used between the cell center and the convection boundary conditions (13, 14). An upwind scheme is adopted to represent advection in the blood vessel domain of Eq. (3). For the transient cases, the convection coefficient, h, used in boundary conditions (13,14) is updated at each time step and the fluid properties used to solve Eqs. (17)–(19) are evaluated at the film temperature T_f of the previous time step. For the steady state solution these properties are evaluated at the film temperature of the previous iteration. Data given in [33] is curve fit for temperature dependence of each fluid property. Variables T, ϕ, and Q_J are solved using an implicit point iterative method. Since it is expected that between time steps dramatic temperature changes occur not over the entire solution domain, but locally within and about the target region, a localized convergence measure is used between iterations. The convergence criterion is defined as $\varepsilon = |T^{p+1}_{i,j,k} - T^{p}_{i,j,k}|$ where p is iteration and convergence is established when $\varepsilon < 10^{-5}$. The value of the convergence parameter,ε, was decreased until the maximum local percent difference (between solutions of decreasing ε value) was less than 1%. Eq. (26) is integrated numerically. Computations were performed on a 3.0 GHz Intel Xeon processor. Typical CPU times were 8–12 h.

5. Results and discussion

To validate the numerical solution, comparisons with analytic solutions were made. The temperature solution of the one-dimensional steady form of Eq. (1) was obtained in the vertical y-direction at a location away from the target region with a prescribed boundary conditions equations (9) and (13) using $h = 700\ \mathrm{W/m^2\,K}$, $T_\infty = 10\ ^\circ\mathrm{C}$, and $T_a = 37\ ^\circ\mathrm{C}$. The one-dimensional solutions of the electric potential and Joule heat equations (22) and (25) are obtained in the horizontal x-direction at the center of the target region ($y = 0$, $z = 5$ mm) without the blood vessel. A SC post-electric breakdown conductivity value of $\sigma_{SC} = 0.01$ S/m is used and the remaining composite tissue conductivity values are the same as in Table 2. Fig. 3 shows good agreement between computed and analytic solutions.

5.1. Electrical solution

The electrical solutions of Eqs. (22) and (25) are found for a DC electroporation pulse with an applied voltage $V_{app} = 400$ V. The distribution of Joule heat is presented in Fig. 4. The area shown is a close-up of the target region in the x–y plane at the axial center of the target region ($z = 5$ mm). In this case the SC is represented at full electroporation breakdown with an electrical conductivity value of $\sigma_{SC} = 0.01$ S/m. The dashed line represents the target region boundary and the dotted lines represent the composite tissue interfaces. The blood vessel is represented by the circle in the center. The symmetry of the Joule heat

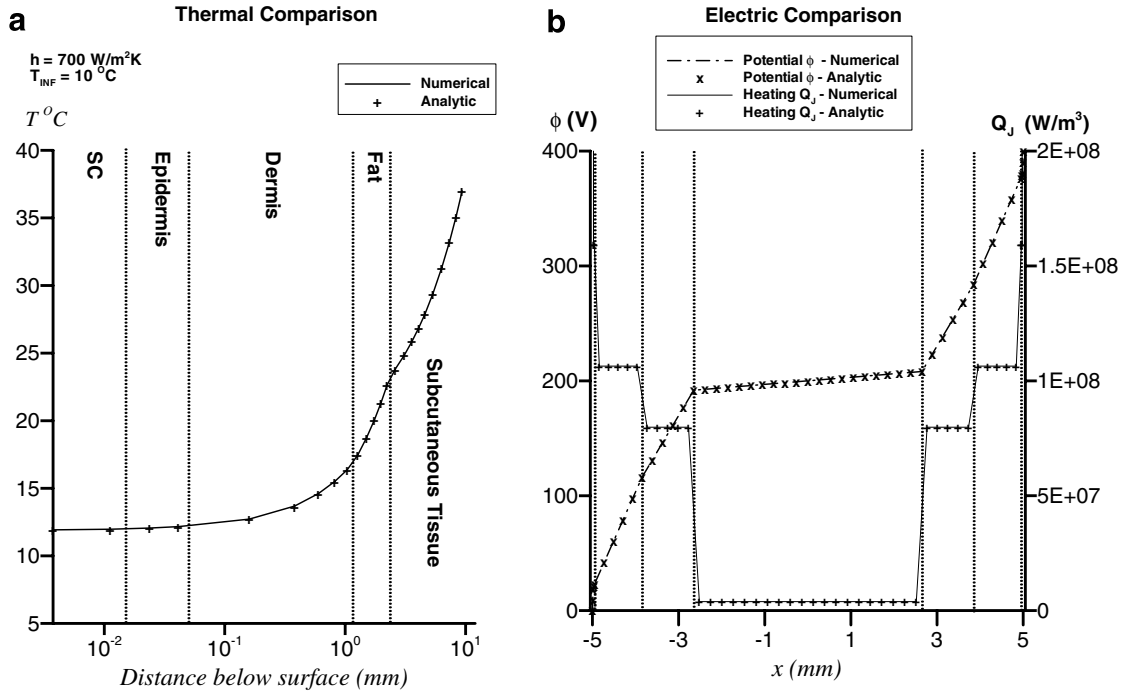

Fig. 3. Comparisons between numerical code and analytic solution (one-dimensional). (a) Steady state temperature (°C), in which the domain represents vertical depth below the skin's surface. (b) Electric (potential and heating) in which the domain represents a horizontal line between the electrodes. Dotted lines separate composite layers.

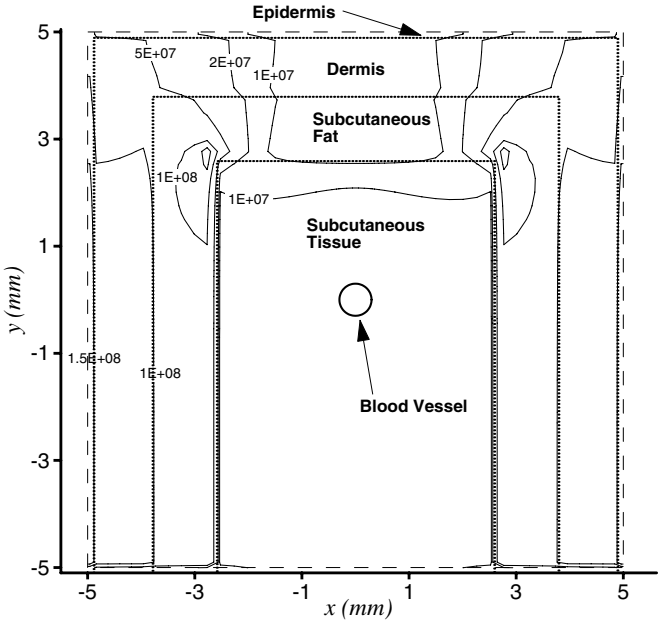

Fig. 4. Joule heat solution (Q_J W/m^3) in the x–y plane at the axial midpoint of the target region ($z = 5$ mm) during an electroporation pulse with an applied potential of 400 V using SC conductivity value ($\sigma_{SC} = 0.01$ S/m). Dotted lines separate composite layers. Dashed line denotes target region boundary.

solution reflects the symmetry of the composite model electrical property values. Large vertical current densities resulting from the non-uniformity of electrical properties of the composite system about the corners of the composite interfaces are implied by the two-dimensional increases in the Joule heat contour values especially about the corners of the fat-dermis interface. In the lower section of the target region (where the composite properties do not change vertically) the contours are predominately one-dimensional in the x-direction with levels of highest heating occurring at locations of lowest tissue electrical conductivity. To gain further insight into the electrical solution variations with respect to composite layer, Fig. 5 shows the electrical solution along the x-axis at the center of the target region ($y = 0$, $z = 5$ mm) for a SC electrical conductivity value of $\sigma_{SC} = 10^{-2}$ S/m. At the blood vessel tissue interface the slight increase in current density is reflected by the increase in Joule heat. The local magnitudes of Joule heat added are in decreasing order SC, epidermis, dermis, fat and subcutaneous muscle tissue, which corresponds to the order of increasing composite conductivity value. The strong one-dimensional tendencies of the potential drops across the composite layers of Fig. 5 are nearly linear, mirroring those of the one-dimensional analytic profile presented in Fig. 3.

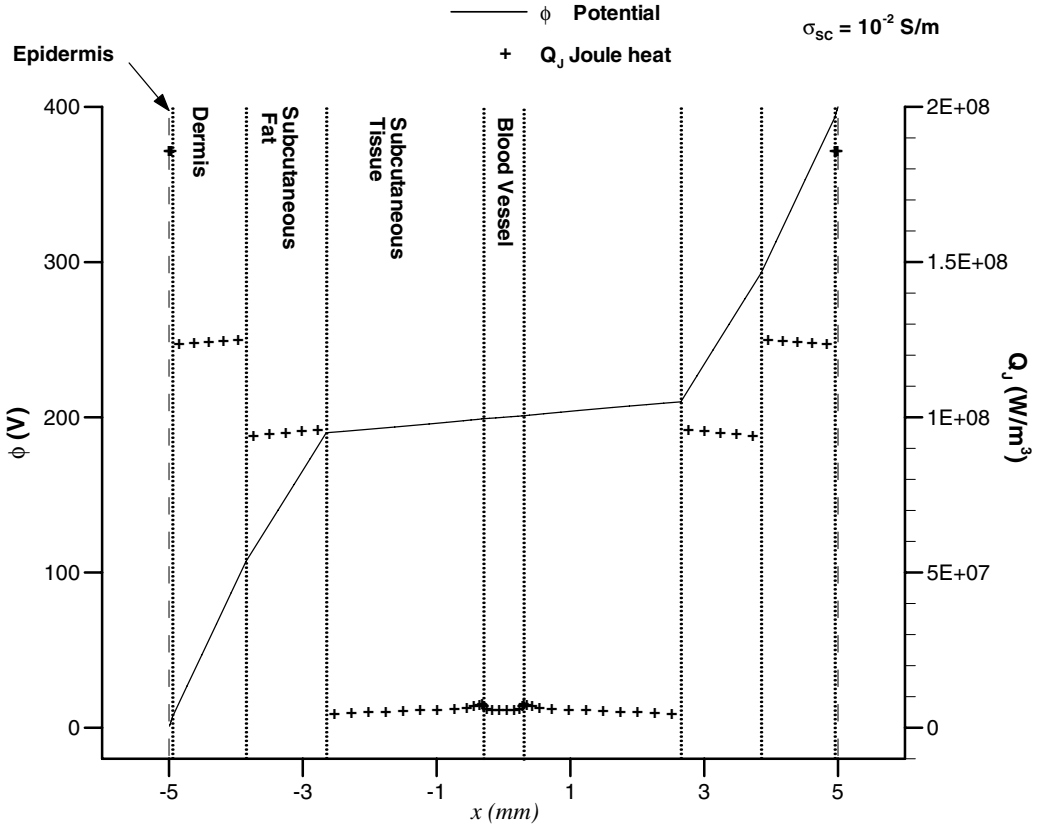

Fig. 5. Composite tissue property effects on electrical solution during electroporation pulse. Solution shown lies between the electrodes at target region vertical and axial midpoints ($y = 0$ mm, $z = 5$ mm). Dotted lines denote interfaces between composite regions, dashed lines denote skin-electrode interfaces, and SC conductivity used denotes post-EP breakdown value.

5.2. Thermal solution

The transient thermal solutions of the electroporation model are now addressed. The electroporation process modeled consists of five 150 ms long DC square wave pulses administered at 1-s intervals with an applied voltage of 400 V. Two representative planes are chosen to depict the thermal and damage solutions: the x–y plane at the axial target region midpoint $z = 5$ mm (Figs. 6–9, 11, 12) and the x–z plane at the blood vessel center $y = 0$ mm (Figs. 8 and 12). Symmetry of the electrical and physical model is utilized so that results are shown only for the positive x half of the model. To model the electrical breakdown of the SC, the conductivity of the SC is assigned a value of $\sigma_{SC} = 10^{-5}$ S/m for the first 5 ms of the first pulse and $\sigma_{SC} = 10^{-2}$ S/m thereafter. Transient thermal contours are shown in Fig. 6 where times shown begin at the end of the last pulse cycle. The maximum temperature contours are presented at $t = 0$ s (immediately after the last pulse cycle of the electroporation process). Recalling the results of the electrical solution it is not surprising to find negligible temperature rise in the least electrically resistive layer, the subcutaneous muscle tissue. From the results depicted in Figs. 4 and 5 it is expected that the maximum temperature rises occur in the SC and epidermal layers, and clearly this is not the case in the thermal solution. To explain this discrepancy it is noted that for each of the 1 Hz pulse cycles, Joule heat is added during the first 150 ms pulse with an 850 ms period remaining during which heat is conducted from the thin 50 μm dermal layer to the thermally conductive electrode. The maximum temperature rises occur along the vertical fat-dermis interface reflects the low specific heat of the fat layer. As time passes, evidence of heat conducted to the electrodes is noticeable by the

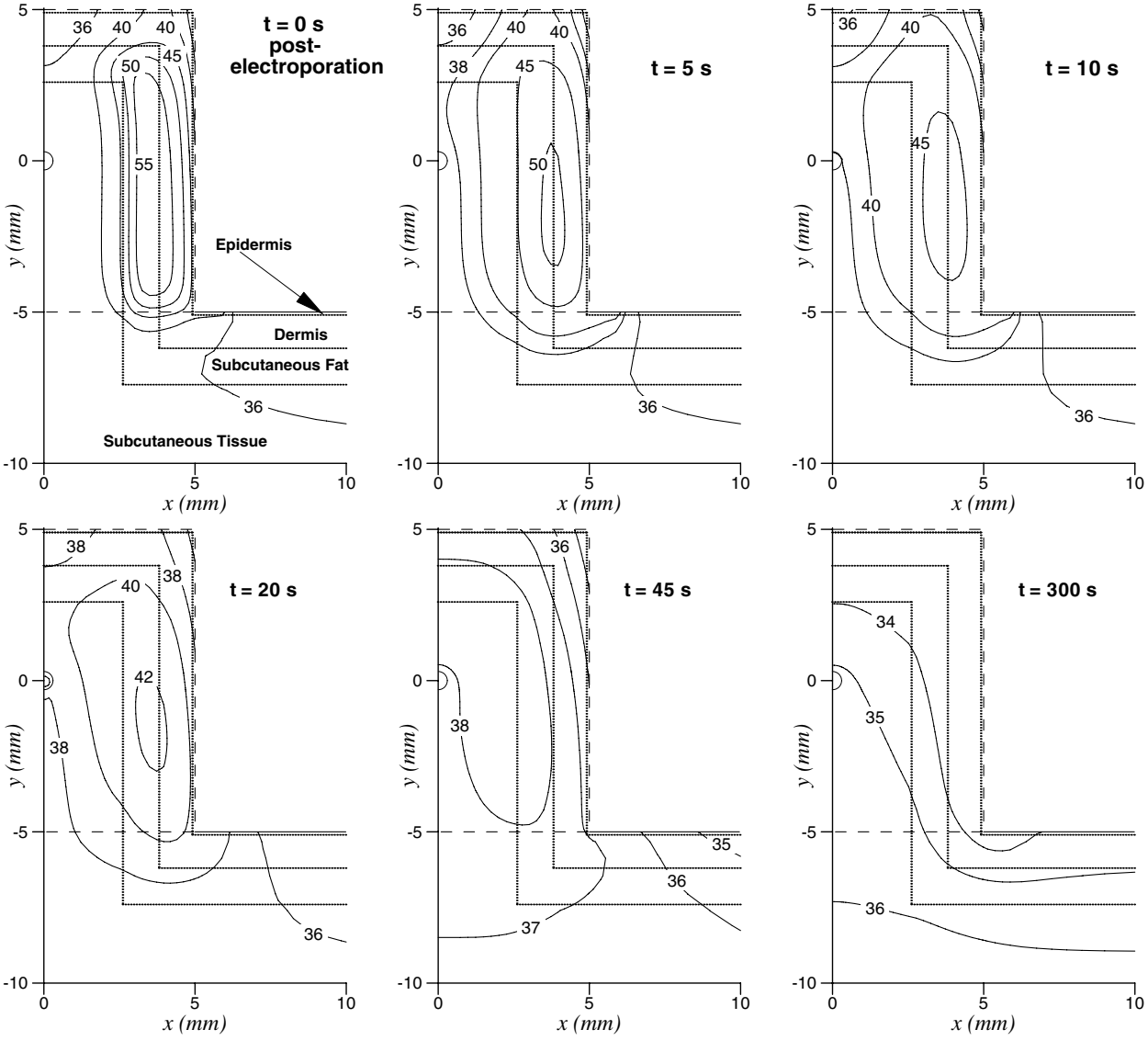

Fig. 6. Post electroporation transient thermal solution (°C) at the target region axial midpoint ($z = 5$ mm). Electroporation consisted of 5 pulses of 150 ms duration spaced 1 s apart with an applied voltage of 400 V. Dotted lines denote interfaces between composite regions, dashed lines denote the target region boundary, and times shown begin after application of the last pulse cycle.

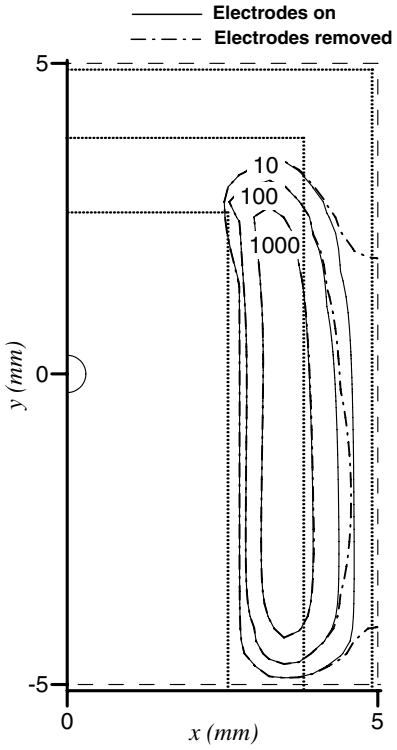

Fig. 7. Electrode effects on thermal damage EM_{43} (min) evaluated at $t = 300$ s (after last pulse cycle) at the axial midpoint of the target region ($z = 5$ mm). Electroporation consisted of 5 pulses 150 ms in duration spaced 1 s apart with an applied voltage of 400 V. Dotted lines denote interfaces between composite regions, dashed lines denote the target region boundary.

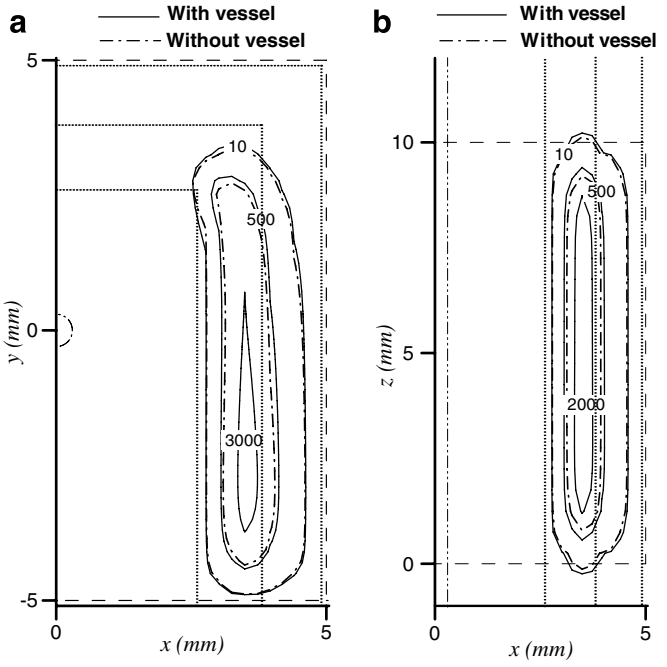

Fig. 8. Blood vessel effects on thermal damage EM_{43} (min) evaluated at $t = 300$ s (after last pulse cycle): (a) the x–y plane at the axial midpoint of the target region ($z = 5$ mm), (b) the x–z plane at the vertical midpoint of the target region ($y = 0$ mm). Electroporation consisted of 5 pulses 150 ms in duration spaced 1 s apart with an applied voltage of 400 V. Dashed line represents target region boundary, dotted lines represent composite tissue interfaces, and dash-dot-dotted line represents position of blood vessel outer radius.

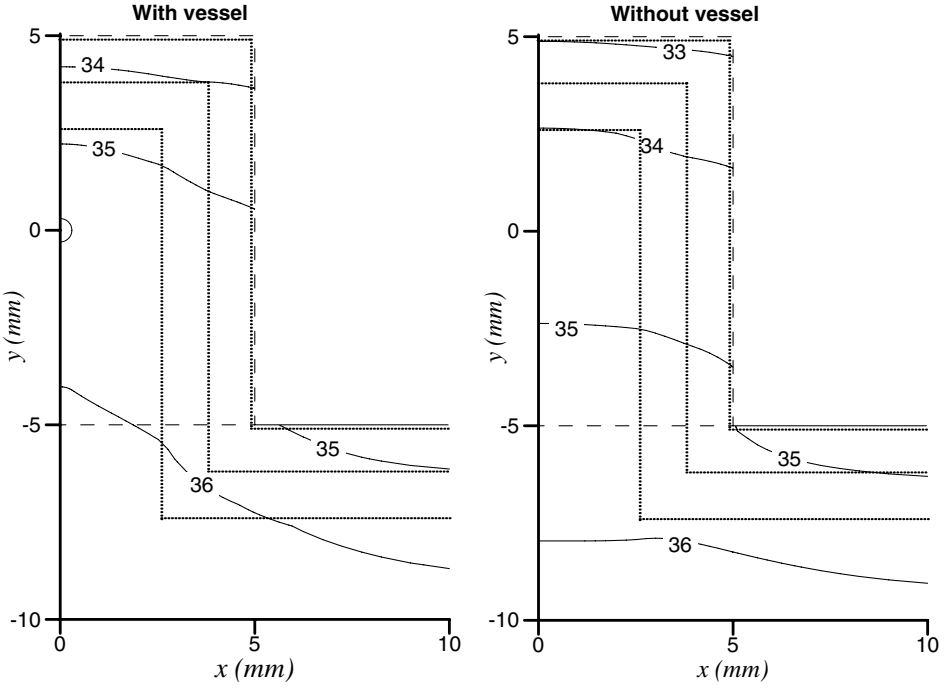

Fig. 9. Blood vessel effects on steady state solution (°C) at the axial midpoint of the target region ($z = 5$ mm). Dashed line represents target region boundary, dotted lines represent composite tissue interfaces.

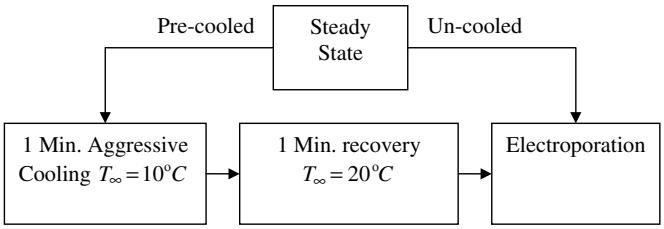

Fig. 10. Cooling technique algorithm.

temperature drop along the tissue-electrode boundary, while the slight vertical temperature variation at the top of the target region shows the much slower rate at which free convection contributes to the cooling. At times less than 45 s the location of highest temperature remains in the vertical center of the target region and about the fat composite layer. At 5 min after the last pulse cycle the temperatures of the target region have reached a level low enough to produce negligible damage. For this reason the thermal damage of Eq. (26) is evaluated from the beginning of the first pulse until 300 *s* after the end of the last pulse cycle.

To get a closer look at the electrode influence, thermal damage comparisons are conducted between the scenario in which the electrodes are removed immediately after the last pulse cycle and one in which the electrodes remain in place during the entire 5 min after electrical pulse. In Fig. 7 the thermal damage solution of both cases yields nearly identical high damage contours about the vertical fat-dermis interface. Recalling the higher temperature contours of Fig. 6, this result is anticipated. However the electrodes' cooling effects are evident in the lower level damage profiles. Post-electroporation electrode removal results in slower cooling of the outer dermis and epidermis composite layer as evidenced by the tendency of lower level damage profiles to extend to the edge of the target region.

Vascular effects are investigated in Fig. 8 for which EM_{43} profiles are shown comparing the cases with and

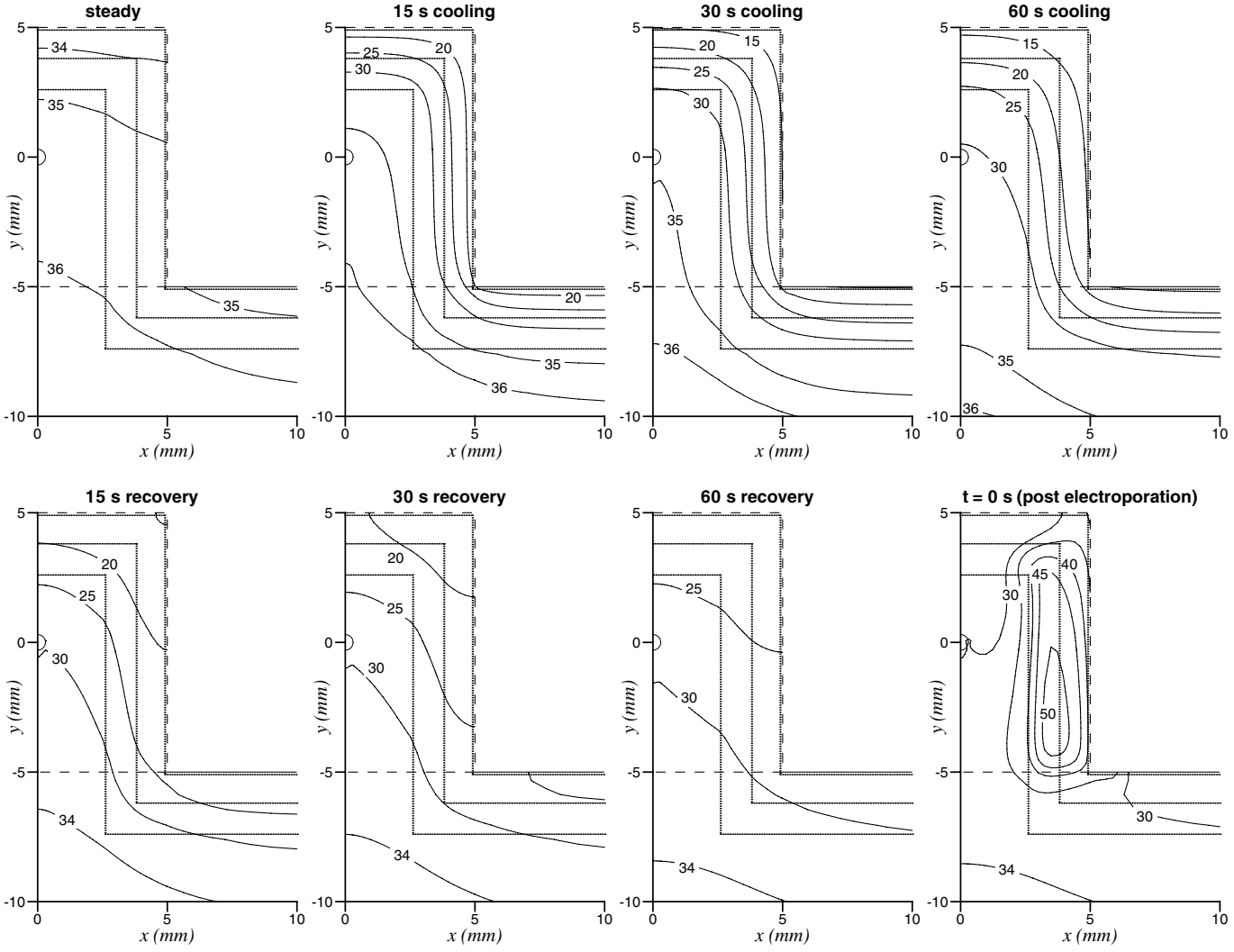

Fig. 11. Transient aggressive cooling and recovery thermal solutions (°C): at the axial midpoint of the target region ($z = 5$ mm), dashed line represents target region boundary, dotted lines represent composite tissue interfaces. Data represented in post-electroporation thermal solution is from an electroporation model consisting of 5 pulses 150 ms in duration spaced 1 s apart with an applied voltage of 400 V.

without the presence of a small blood vessel. The low and moderate level contours are primarily very similar, which suggests no direct interaction between the heated fat-dermis interface and the blood vessel. In this case the two are separated by a distance of nearly 3 mm. However an unanticipated result is seen in both the x–z and x–y planes which clearly shows that the case with the blood vessel reaches a greater maximum thermal damage value; the blood vessel acts to add heat to the target region. A comparison between steady state solutions of Fig. 9 shows that the blood vessel advects heat into the target region slightly raising the steady state temperature uniformly. Recalling that the steady state solutions are used as initial conditions, it follows that the maximum temperature achieved during electroporation is slightly higher for the blood vessel case. Because the vessel adds heat to the muscle tissue, the conduction of heat to from the high temperature fat layer into to the muscle tissue is inhibited. This results in a slower cooling of the high temperature region which explains the associated higher maximum damage values.

5.3. Aggressive cooling technique

The sensitivity of thermal damage found from the results of Figs. 8 and 9 prompted the authors to conduct a theoretical exercise. If the small elevated temperature associated with the vessel greatly contributes to total thermal damage, should not the reverse hold true as well? An aggressive cooling technique is proposed in which the temperature of the target region is reduced by exposing the model forearm to a cold water bath at $T_\infty = 10\,^\circ\mathrm{C}$ for 1 min (water properties are used in Eqs. (13) and (17)–(19). Then a recovery time period of 1 min is allowed in which the tissue is exposed to the ambient air at $T_\infty = 10\,^\circ\mathrm{C}$ (air properties are used in Eqs. (13) and (17)–(19)). This recovery time is added primarily to model the time period during which an experimentalist would prepare the target region site prior to the application of the electrodes. Immediately following the recovery period, the electrodes are modeled in place and the electroporation pulse cycles are administered. A representative flow diagram of the procedure is given in Fig. 10. Fig. 11 shows the temperature profiles during aggressive cooling and subsequent recovery heating as well as the maximum temperature profile of the system following electroporation. Noting the difference in temperature profiles just prior to electroporation (60 s recovery for the pre-cooled case and steady state for the un-cooled case) it is not surprising that after electroporation, high temperature profiles associated with the cooling technique (seen at $t = 0$ s of Fig. 11) are nearly 5 °C lower than those of the un-cooled case depicted in Fig. 6. Comparing the pre-cooled thermal damage profiles of Fig. 12 to those of the un-cooled profiles of Fig. 8, it is obvious that using an aggressive cooling technique results in much lower thermal damage. Cooling the target region prior to electroporation results in a lower maximum temperature and greatly reduces the risk of thermal damage.

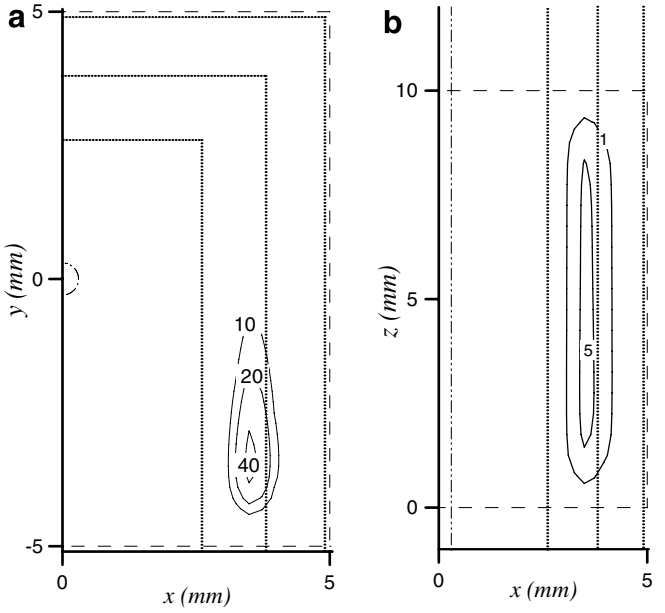

Fig. 12. Aggressive cooling results showing reduced thermal damage EM_{43} (min) at $t = 300$ s (after last pulse cycle): (a) the x–y plane at the axial midpoint of the target region ($z = 5$ mm), (b) the x–z plane at the vertical midpoint of the target region ($y = 0$ mm); Dashed line represents target region boundary, dotted lines represent composite tissue interfaces, and dash-dot-dotted line represents position of blood vessel. Electroporation consisted of 5 pulses 150 ms in duration spaced 1 s apart with an applied voltage of 400 V.

It should be noted that reduced perfusion associated with decreased skin surface temperature resulting in slower cooling is not modeled in this study, which means that in practice greater aggressive cooling is required to lower target region temperature. Furthermore in this study during the cooling the physical model represented the raised configuration of Fig. 1. In practice the target region may not be raised during cooling which results in a lower convection influence. Again to achieve similar target region temperatures, in practice greater cooling requirements are expected.

6. Conclusions

A transient three-dimensional model of *in vivo* skin electroporation representing the composite layers of the skin has been developed in which electrical and transient thermal solutions are found. The electrical solution of the skin composite model shows a strong one-dimensional tendency parallel to the induced electric field. The highly electrically resistive SC and epidermis layers receive the largest Joule heating, while in the more conductive subcutaneous muscle tissue heating is negligible. The dermis and subcutaneous fat layers are at great risk of thermal damage. A blood vessel running deep in the subcutaneous muscle tissue indirectly increases the maximum value of thermal damage by adding heat to the target region. Leaving the electrodes attached to the skin after electroporation promotes cooling, thereby reducing thermal damage of the outer composite layers. This promotes research directed towards increasing the cooling

capacity of electroporation calipers. Effectively cooling tissue prior to electroporation reduces the risk of thermal damage, allowing the experimentalist to use pulse parameters which increase the likelihood of successful drug delivery.

Acknowledgements

The authors express gratitude to the North Carolina Space Grant Consortium and the National Space Grant College and Fellowship Program for financial support contributing to this work.

References

[1] L.M. Mir, Therapeutic perspectives of in vivo cell elecropermeabilization, Bioelectrochemistry 53 (2000) 1–10.
[2] S. Orlowski, L.M. Mir, Cell electropermeabilization: a new tool for biochemical and pharmacological studies, Biochim. Biophys. Acta 1154 (1993) 51–63.
[3] J. Gehl, Electroporation: theory and methods, perspectives for drug delivery, gene therapy and research, Acta. Physiol. Scand. 177 (2003) 437–447.
[4] J.C. Weaver, Electroporation: a general phenomenon for manipulating cells and tissue, J. Cell. Biochem. 51 (1993) 426–435.
[5] J.C. Weaver, Electroporation of cells and tissues, IEEE Trans. Plasma Sci. 28 (2000) 24–33.
[6] U.F. Pliquet, C.A. Gusbeth, Perturbation of human skin due to application of high voltage, Bioelectrochemistry 51 (2000) 41–51.
[7] M.R. Prausnitz, The effects of electric current applied to the skin: a review for transdermal drug delivery, Adv. Drug Deliv. Rev. 18 (1996) 395–425.
[8] U.F. Pliquet, T.E. Zewert, T. Chen, R. Langer, J.C. Weaver, Imaging of fluorescent molecule and small ion transport through human stratum corneum during high voltage pulsing: localized transport regions are involved, Biophys. Chem. 58 (1996) 185–204.
[9] M.R. Prausnitz, Do high voltage pulses cause changes in skin structure? J. Controlled Release 40 (1996) 321–326.
[10] U.F. Pliquet, R. Langer, J.C. Weaver, Changes in the passive electrical properties of human stratum corneum due to electroporation, Biochim. Biophys. Acta 1239 (1995) 111–121.
[11] R. Vanbever, R. Pleat, In vivo efficacy and safety of skin electroporation, Adv. Drug Deliv. Rev. 35 (1999) 77–88.
[12] R. Vanbever, G. Langers, S. Montmayeur, V. Preat, Transdermal delivery of fentanyl: rapid onset of analgesia using skin electroporation, J. Controlled Release 50 (1998) 225–235.
[13] R. Vanbever, E. LeBoulenge, V. Preat, Transdermal delivery of fentanyl by electroporation: I. Influence of electrical factors, Pharm. Res. 13 (1996) 559–565.
[14] R. Vanbever, U.F. Pliquett, V. Preat, J.C. Weaver, Comparison of the effects of short, high-voltage and long, medium-voltage pulses on skin electrical and transport properties, J. Controlled Release 60 (1999) 36–47.
[15] A.R. Denet, R. Vanbever, V. Preat, Skin electroporation for transdermal and topical delivery, Adv. Drug Deliv. Rev. 56 (2004) 659–674.
[16] M.R. Prausnitz, V.G. Bose, R. Langer, J.C. Weaver, Electroporation of mammalian skin: a mechanism to enhance transdermal drug delivery, P. Natl. Acad. Sci. USA 90 (1993) 10504–10508.
[17] T. Suzuki, B. Shin, K. Fujikura, T. Matsuzaki, K. Takata, Direct gene transfer into rat liver cells by electroporation, FEBS Lett. 425 (1998) 436–440.
[18] T. Muramatsu, A. Nakamura, H. Park, In vivo electroporation: a powerful and convenient means of nontrivial gene transfer to tissues of living animals, Int. J. Mol. Med. 1 (1998) 55–62.
[19] R.V. Davalos, L.M. Mir, B. Rubinsky, Tissue ablation with irreversible electroporation, Annals Biomed. Eng. 33 (2005) 223–231.
[20] R.V. Davalos, B. Rubinsky, L.M. Mir, Theoretical analysis on the thermal effects during in vivo tissue electroporation, Bioelectrochemistry 61 (2003) 99–107.
[21] S.M. Becker, A.V. Kuznetsov, Numerical modeling of in vivo plate electroporation thermal dose assessment, J. Biomech. Eng. T ASME 128 (2006) 76–84.
[22] S.M. Becker, A.V. Kuznetsov, Numerical assessment of thermal response associated with in vivo skin electroporation: the importance of the composite skin model, J. Biomech. Eng. T ASME, *in review*.
[23] P.F. Millington, R. Wilkinson, Skin, Cambridge University Press, Cambridge, Great Britain, 1983.
[24] H.H. Pennes, Analysis of tissue and arterial blood temperatures in the resting forearm, J. Appl. Physiol. 1 (1948) 93–122.
[25] J. Gehl, T. Skovsgaard, L.M. Mir, Vascular reactions to in vivo electroporation: characterization and consequences for drug and gene delivery, Biochim. Biophys. Acta 1569 (2002) 51–58.
[26] T.C. Shih, H.S. Kou, W.L. Lin, The impact of thermally significant blood vessels in perfused tumor tissue on thermal dose distributions during thermal therapies, Int. Comm. Heat Mass Transfer 30 (2003) 975–985.
[27] L.O. Svaasand, L.L. Randeberg, G. Aguilar, B. Majaron, S. Kimel, E.J. Lavernia, J.S. Nelson, Cooling efficiency of cryogen spray during laser therapy of skin, Laser Surg. Med. 32 (2003) 137–142.
[28] F.A. Duck, Physical Properties of Tissue: A Comprehensive Reference Book, Academic Press, London, 1990.
[29] S.B. Wilson, V.A. Spence, A tissue heat transfer model for relating dynamic skin temperature changes to physiological parameters, Phys. Med. Biol. 8 (1988) 895–912.
[30] J.C. Chato, R.C. Lee, The future of biothermal engineering, Ann. NY Acad. Sci. 858 (1998) 1–20.
[31] F.M. Hendriks, D. Brokken, C.W.J. Oomens, F.P.T. Baaijens, Influence of hydration and experimental length scale on the mechanical response of human skin in vivo, using optical coherence tomography, Skin Res. Technol. 10 (2004) 231–241.
[32] P. Wainwright, Thermal effects of radiation from cellular telephones, Phys. Med. Biol. 45 (2000) 2363–2372.
[33] A. Bejan, Heat Transfer, Wiley, New York, 1993.
[34] S. Gabriel, R.W. Lau, C. Gabriel, The dielectric properties of biological tissues: II. Measurements in the frequency range 10 Hz to 20 GHz, Phys. Med. Biol. 41 (1996) 2251–2269.
[35] Y.A. Chizmadzhev, A.V. Indenbom, P.I. Kuzmin, S.V. Galichenko, J.C. Weaver, R.O. Potts, Electrical properties of skin at moderate voltages: contribution of appendageal macropores, Biophys. J. 74 (1998) 843–856.
[36] L. Tung, Detrimental effects of electrical fields on cardiac muscle, Proc. IEEE 84 (1996) 366–378.
[37] Y. Kim, H.G. Zieber, F.E. Wang, Uniformity of current density under stimulating electrodes, Crit. Rev. Biomed. Eng. 17 (1990) 585–619.
[38] S.A. Sapareto, W.C. Dewey, Thermal dose determination in cancer therapy, Int. J. Rad. Onc. Biol. Phys. 10 (1984) 787–800.
[39] M.W. Dewhirst, B.L. Viglianti, M. Lora-Michiels, M. Hanson, P.J. Hoopes, Basic principles of thermal dosimetry and thermal thresholds for tissue damage from hyperthermia, Int. J. Hyperthermia 19 (3) (2003) 267–294.
[40] S.J. Graham, L. Chen, M. Leitch, R.D. Peters, M.J. Bronskill, F.S. Foster, R.M. Henkelman, D.B. Plewes, Quantifying tissue damage due to focused ultrasound heating observed by MRI, Magnet. Reson. Med. 41 (1999) 321–328.
[41] S.V. Patankar, Numerical Heat Transfer and Fluid Flow, Hemisphere, Washington DC, 1980.